Proceedings of ICRC 2001: 2231 © Copernicus Gesellschaft 2001

ICRC 2001

The Energetic Trans-Iron Composition Experiment (ENTICE) on the Heavy Nuclei eXplorer (HNX) Mission

M. H. Israel[1], J. H. Adams[2], L. M. Barbier[3], W. R. Binns[1], E. R. Christian[3], N. Craig[4], A. C. Cummings[5], J. R. Cummings[1], T. Doke[6], N. Hasebe[6], T. Hayashi[6], D. Lee[7], R. A. Leske[5], D. Mark[7], R. A. Mewaldt[5], J. W. Mitchell[3], K. Ogura[8], S. M. Schindler[5], E. C. Stone[5], G. Tarlé[9], H. Tawara[10], C. J. Waddington[11], A. J. Westphal[4], M. E. Wiedenbeck[12], and N. Yasuda[13]

[1]Washington University in St. Louis
[2]NASA/Marshall Space Flight Center
[3]NASA/Goddard Space Flight Center
[4]University of California, Berkeley
[5]California Institute of Technology
[6]Waseda University
[7]Swales Aerospace
[8]Nihon University
[9]University of Michigan
[10]KEK
[11]University of Minnesota
[12]Jet Propulsion Laboratory
[13]National Institute of Radiological Sciences, Japan

Abstract. The HNX mission is composed of the ENTICE and ECCO experiments. The experimental goal of ENTICE is to measure with high precision the elemental abundances of all nuclei with 10≤Z≤82. This will enable us to determine if the injection mechanism for the cosmic ray accelerator is controlled by FIP or Volatility and to study the mix of nucleosynthetic processes that contribute to the galactic cosmic ray source. The ENTICE experiment utilizes the dE/dx-C method of charge determination and consists of silicon dE/dx detectors, Cherenkov detectors with two different refractive indices, and a fiber hodoscope. We will describe the instrument and its performance based on beam tests of a prototype instrument.

1. Introduction

The ENTICE experiment is one of two instruments that make up the HNX mission (Binns et al. and Westphal et al., this conference). The ENTICE instrument utilizes three detector subsystems (silicon detector arrays, a Cherenkov module, and a trajectory detector) to unambiguously measure the charge (Z) of all GCRs heavier than neon having energy greater than ~500MeV/nucleon at the top of the instrument. Figure 1 is a cross-sectional drawing of the instrument.

On top and bottom of ENTICE are arrays of silicon detectors that measure the incident particle's rate of energy loss, dE/dx, which is dependent on Z and velocity. Just inboard of each silicon array is a scintillating fiber detector that measures the trajectory of particles traversing the instrument. In the middle of the detector stack are two Cherenkov counters, which measure the Cherenkov light emitted by the particle as it traverses the radiator in each counter. The total amount of Cherenkov light produced is also a function of Z and velocity. The upper Cherenkov counter contains an aerogel radiator with refractive index ~1.04, corresponding to a threshold energy for emission of Cherenkov radiation of ~2.5GeV/nucleon. The lower Cherenkov counter contains an acrylic radiator with refractive index of 1.49, and has a threshold energy of ~0.3 GeV/nucleon. These radiators are contained in light diffusion boxes, with each box being viewed by 48 five-inch photo-multiplier tubes (PMTs). By combining these measurements, the charge of incident GCRs can be unambiguously determined. For GCRs with energy between ~0.5 and ~7GeV/nucleon, the particle's energy is also determined.

Correspondence to:M. Israel (mhi@wuphys.wustl.edu)

2. Charge Identification Technique

The particle's charge is identified by a combination of dE/dx and Cherenkov measurements, with the trajectory being used to correct signals for the angle of incidence and for area non-uniformities in the detector response. The primary reason for using two Cherenkov counters with different refractive indices is to resolve the ambiguity in charge identification that occurs in a simple dE/dx vs. Cherenkov measurement due to relativistic rise in ionization. The ratio of the two Cherenkov signals determines three energy regions. In region 1, below the $C_{1.04}$ threshold, the charge identification (Fig. 2a) is based on dE/dx and $C_{1.49}$. Region 2, with intermediate values of $C_{1.04}/C_{1.49}$, has 2.5≤E≤6.3 GeV/nucleon; there charge identification (Fig. 2b) is based on dE/dx with a small velocity correction from $C_{1.04}$. Region 3, with high values of $C_{1.04}/C_{1.49}$, has E≥6.3 GeV/nucleon; there charge identification (Fig. 2c) is based on $C_{1.49}$ and dE/dx. The relativistic rise in the silicon detectors is not as dramatic as shown in Figure 2c due to the restricted energy loss in these thin detectors.

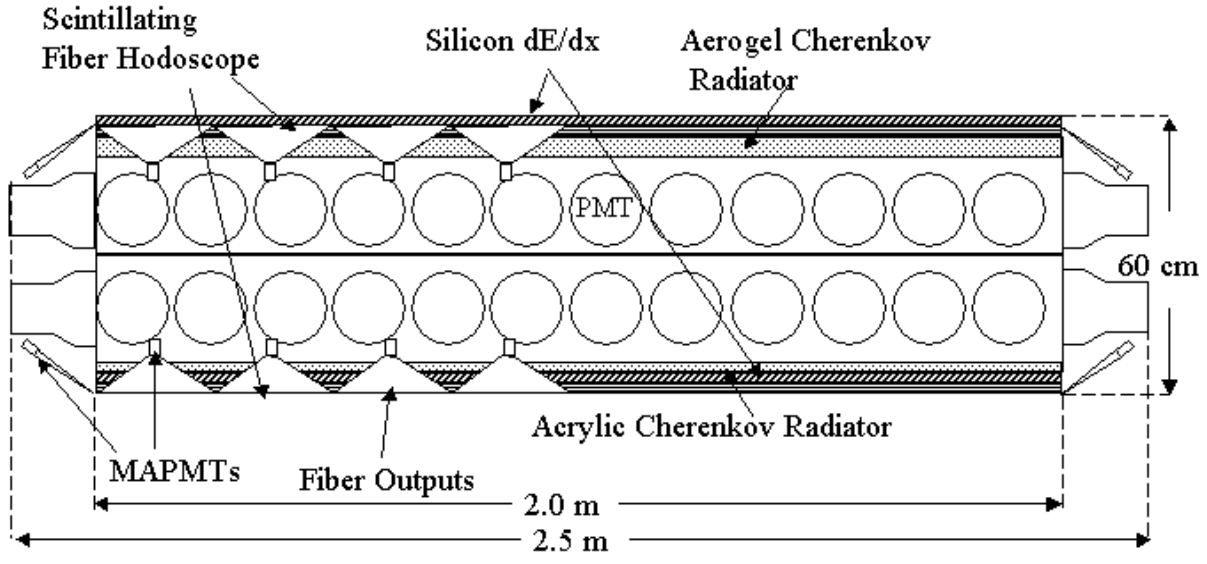

FIGURE 1. ENTICE Cross-sectional view

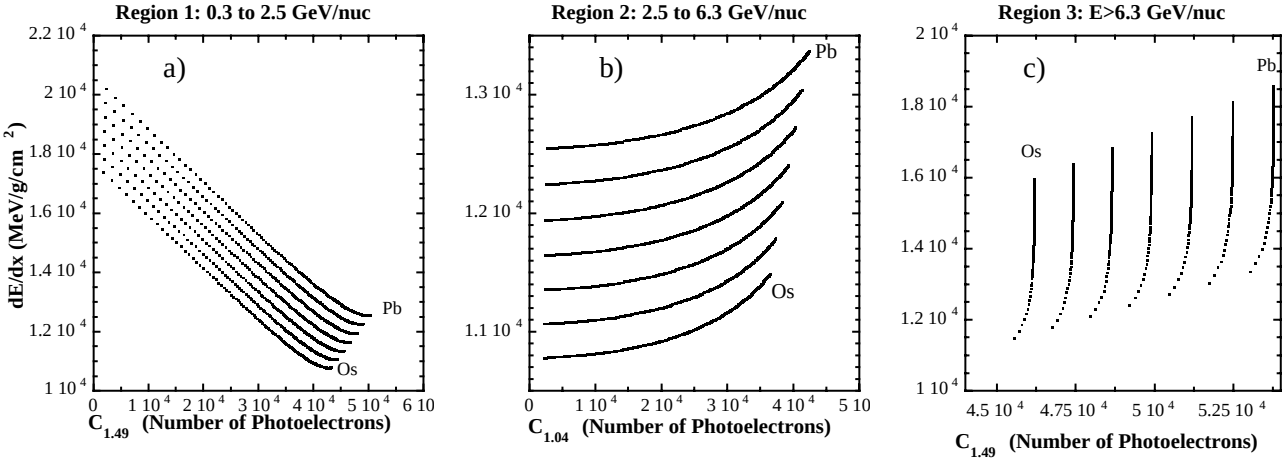

FIGURE 2-Charge identification method

3. Detector Systems

Silicon Array--Two close-packed mosaics of silicon diodes cover areas of 2x2 m^2 at the top and bottom of the sensor stack. The individual detectors that make up each of these layers are square, ion-implanted devices with nominal thickness 380 microns and a single large-area contact. Each array is composed of 100 detector tiles each having 400 cm^2 of detectors, either four ~10 cm square detectors or nine ~6.6 cm square detectors. The total number of detectors needed for flight is in the range 800 to 1800, depending on the selected detector size. The charge signals from all detectors in a tile are combined into two signals for readout. A carbon fiber reinforced polymer frame designed to minimize inactive area supports the tiles.

The detector signals are processed with a custom VLSI circuit for which we have baselined the chip that was developed for the SIS instrument flown on ACE. Tests are planned on these VLSI circuits to verify their performance for the ENTICE silicon detectors.

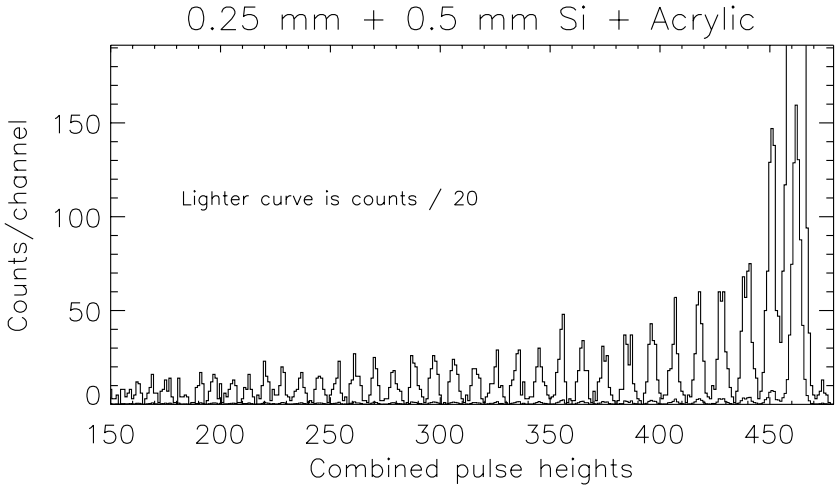

FIGURE 3—Resolution obtained for gold nuclei (Z=79) and fragments at 10.6 GeV/nuc using a weighted sum of silicon and acrylic Cherenkov signals. The largest peak on the right is the gold peak and the fragment peaks extend to the left.. The lighter curve is the number of counts divided by 20.

The charge resolution achievable for high-energy, ultraheavy (UH) nuclei by combining signals from two silicon layers with total thickness 750 microns and the acrylic Cherenkov signal is shown in Fig. 3. These data are from a test run made with a beam of 10.6 GeV/nuc gold nuclei (Z=79) from the AGS accelerator at Brookhaven National Laboratory. The beam was fragmented upstream of the detectors to obtain a spectrum of charges. Note that in Figure 3 the peak corresponding to $_{79}$Au (dark line) goes off scale to more clearly display the resolution of the gold fragments. The measured charge resolution of $\sigma_Z \leq 0.20e$ is sufficient to clearly resolve individual elements in the Pt-Pb region of the charge spectrum. We also note that $_{78}$Pt, which has a peak height that is only 4% that of the neighboring $_{79}$Au peak, is clearly resolved.

By requiring consistency between the pulse heights from the two silicon detectors it will be possible to efficiently remove background events in which the incident particle fragments within the instrument. To optimize the charge resolution, detector thickness will be mapped using the large sample of high-energy iron nuclei collected in flight. We will obtain ~2000 Fe nuclei/cm^2 of detector area, enabling us to obtain precise response maps on small scales.

Cherenkov Module--The Cherenkov module consists of two light diffusion boxes, acrylic and aerogel radiators, five-inch PMTs and the PMT front-end electronics. The Cherenkov light boxes are each made with four machined aluminum side-walls. The top of the aerogel light box and the bottom of the acrylic light box have low density structural supports, such as carbon-fiber faced Rohacell or poly-honeycomb to provide stiffness for the light box assemblies and support for the radiators. The interior of the light boxes will be lined with a diffuse reflector such as Tyvek^{TM}.

The acrylic Cherenkov radiator is 1.27 cm thick and the radiator surfaces are bead blasted to produce diffuse emission. The acrylic also has 20 mg/liter of Bis-MSB waveshifter added to shift the ultraviolet light into the blue. This is a higher concentration of waveshifter dye than is commonly used. This increases the fraction of Cherenkov light that is waveshifted before leaving the radiator and should reduce the directionality of light that is collected by the phototubes. The light output obtained with a prototype detector having a 1.27 cm thick, 1.15m square radiator, the same light box height to width aspect ratio, and the same photocathode-to-light box surface area as the ENTICE detector, was 16 photoelectrons (pe) per minimum-ionizing particle (MIP). The Acrylic Cherenkov charge resolution obtained at BNL for fragmented 10.6GeV/nuc $_{79}$Au is $\sigma_Z = 0.23e$.

The aerogel radiator consists of a mosaic of close packed blocks having nominal dimensions of 40cm square and 3cm thick. The light yield from a prototype detector (similar to the acrylic prototype described above) was ≥3pe per MIP. The energy response of the prototype detector is shown in Fig. 4 where we have plotted the Aerogel signal vs the Acrylic signal. The points represent the mean signal for gold nuclei for energies ≤10.6 GeV/nuc and the error bars represent the width of the signal

distribution for gold nuclei. We see the sharp turn on of the Aerogel near its Cherenkov threshold that is used to discriminate between low energy and high energy nuclei (Cummings et al., 1999). The response of both the Aerogel and Acrylic Cherenkov prototype detectors meet the requirements for ENTICE.

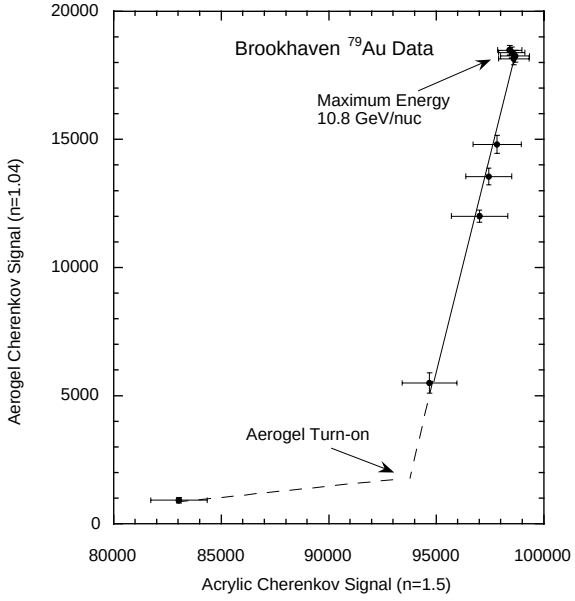

Figure 4—The signal from the Aerogel Cherenkov counter is plotted vs. the Acrylic Signal for gold nuclei with energies ≤10.6 GeV/nuc.

Trajectory Detector--The Trajectory Detector subsystem consists of 32 identical scintillating fiber panels, each panel consisting of 500 0.5mm square cross-section scintillating fibers coupled on each end to a 16-channel multi-anode photomultiplier tube (MAPMT) and mounted on a 25cm wide by 200cm long aluminum substrate. Eight of these panels form one layer (a single coordinate) of the trajectory detector.

The Hamamatsu R-5900-M16 16-anode MAPMT is planned for the hodoscope fiber readout (Rielage, et al., 2001). By coding the fiber outputs on either end of the panel (Lawrence et al., 1999) we can unambiguously determine which of the 256 1-mm section of fibers the particle passed through using 32 anodes, 16 on either end of the fiber panel. A prototype coded trajectory detector was successfully tested at BNL using 1 mm fibers. Resolution better than 1 mm was obtained as described in Cummings, et al., 1999. Additionally, we have successfully used a coded fiber hodoscope on the TIGER instrument (Sposato, et al., 2000) We have performed successful environmental tests on the 64-anode version of this MAPMT, including vibration tests of 7 devices and thermal/vacuum tests over the range –35°C to +40°C. The MAPMT readout will be accomplished with an Application Specific Integrated Circuit (ASIC). We are considering an ASIC developed as part of GLAST technology development that has all the features required for ENTICE with a nominal power of 0.3mW/channel. We will also consider the ACE-VLSI circuit used for silicon detector readout as an option for the MAPMT readout.

4. Summary

We have shown that the ENTICE instrument is capable of the precise charge resolution required to measure the abundances of all nuclei with $10 \le Z \le 83$. The combination of ECCO, with its large collecting power, and ENTICE, which will, in addition to measuring abundances of nuclei up through Z=83, provide a reference of the UH nuclei to iron, should enable us to obtain for the first time a comprehensive table of the abundances of all ultra-heavy galactic cosmic ray elements.

Acknowledgements. This research was supported in part by the National Aeronautics and Space Administration under grant NAG5-10802 and by the McDonnell Center for the Space Sciences at Washington University.

References

Binns, W. R., et al., (1989) *ApJ*, **346**, 997.

Cummings, J.R., et al., (1999) *26th ICRC Proc*., **5**, 156

Lawrence, D.J. et al, (1999) NIM-A **420**, 402.

Rielage, K., et al., (2001) NIM-A, **463**, 149.

Sposato, S.H., et al., (2000) in *Acceleration and Transport of Energetic Particles Observed in the Heliosphere: ACE 2000 Symposium,Ed. R.A. Mewaldt, et al., p433.*